ARL-TR-7328 ● JUN 2015

US Army Research Laboratory

The Use of Compressive Sensing to Reconstruct Radiation Characteristics of Wide-Band Antennas from Sparse Measurements

by Patrick Debroux and Berenice Verdin

NOTICES

Disclaimers

The findings in this report are not to be construed as an official Department of the Army position unless so designated by other authorized documents.

Citation of manufacturer's or trade names does not constitute an official endorsement or approval of the use thereof.

Destroy this report when it is no longer needed. Do not return it to the originator.

ARL-TR-7328 ● JUN 2015

US Army Research Laboratory

The Use of Compressive Sensing to Reconstruct Radiation Characteristics of Wide-Band Antennas from Sparse Measurements

by Patrick Debroux and Berenice Verdin
Survivability/Lethality Analysis Directorate, ARL

REPORT DOCUMENTATION PAGE	Form Approved OMB No. 0704-0188

1. REPORT DATE *(DD-MM-YYYY)*	2. REPORT TYPE	3. DATES COVERED (From - To)
June 2015	Final	January–April 2015

4. TITLE AND SUBTITLE	5a. CONTRACT NUMBER
The Use of Compressive Sensing to Reconstruct Radiation Characteristics of Wide-Band Antennas from Sparse Measurements	5b. GRANT NUMBER
	5c. PROGRAM ELEMENT NUMBER

6. AUTHOR(S)	5d. PROJECT NUMBER
Patrick Debroux and Berenice Verdin	5e. TASK NUMBER
	5f. WORK UNIT NUMBER

7. PERFORMING ORGANIZATION NAME(S) AND ADDRESS(ES)	8. PERFORMING ORGANIZATION REPORT NUMBER
US Army Research Laboratory ATTN: RDR-SLE-E White Sands Missile Range, NM 88002-5513	ARL-TR-7328

9. SPONSORING/MONITORING AGENCY NAME(S) AND ADDRESS(ES)	10. SPONSOR/MONITOR'S ACRONYM(S)
	11. SPONSOR/MONITOR'S REPORTNUMBER(S)

12. DISTRIBUTION/AVAILABILITY STATEMENT

Approved for public release; distribution unlimited.

13. SUPPLEMENTARY NOTES

14. ABSTRACT

Characterization measurements of wide-band antennas can be time intensive and expensive as many data points are required both in the angular and the frequency dimensions. Compressive sensing is proposed to reconstruct the radiation patterns and frequency behavior of antennas from a sparse and random data set of measurements. Parallel compressive sensing is used to reconstruct the desired 2-dimensional (2-D) far-field, radiation-frequency pattern from a randomly distributed, limited set of measurements. Three antenna models were constructed—a pyramidal horn, a Vivaldi, and a bicone—and their 2-D far-field radiation patterns were modeled over a large frequency range using a high-frequency structural simulator. Analyses of uniform- versus nonuniform-pattern reconstruction, of transform function used, and of minimum randomly distributed measurements needed to reconstruct the antennas' radiation characteristics showed the radiation-frequency patterns of the 3 antennas are better reconstructed with the discrete Fourier transform in the angular dimension and with the discrete cosine transform in the frequency dimension. Further, little difference was found in the radiation-frequency pattern's reconstruction using uniform and nonuniform randomly distributed samples even though the pattern error manifests itself differently. The radiation-frequency patterns of the 3 antennas were adequately reconstructed using as little as 30% of calculated points.

15. SUBJECT TERMS

Antenna measurement, antenna radiation pattern, signal reconstruction, compressive sensing

16. SECURITY CLASSIFICATION OF:			17. LIMITATION OF ABSTRACT	18. NUMBER OF PAGES	19a. NAME OF RESPONSIBLE PERSON
a. REPORT	b. ABSTRACT	c. THIS PAGE	UU	28	Patrick Debroux
Unclassified	Unclassified	Unclassified			19b. TELEPHONE NUMBER (Include area code) (575) 678-5238

Contents

List of Figures

INTENTIONALLY LEFT BLANK.

1. Introduction

The measurement of wide-band antennas is often a long and expensive process requiring substantial antenna range time to measure the radiated fields at all angles and all frequencies under consideration. An identified need has been for a method to adequately characterize the radiation pattern of wide-band antennas using fewer measurement points. This need is greater when antennas are characterized over a large frequency bandwidth where an antenna's radiation pattern must be measured at intervals of the frequency range.

Characterization data compactness has been achieved using model-based parameter estimation (MBPE) described by Miller,[1] which approximates the far-field radiation pattern using a simple antenna model and then augments and calibrates the model's results using sparse measurements. Research has been conducted using MBPE to interpolate the antenna's radiated fields in both the spatial and spectral domains so that changes in radiation pattern with frequency can also be extrapolated.[2] The MBPE method is not completely empirical as the antenna must be modeled, albeit in rudimentary fashion, to allow proper interpolation. Martí-Canales et al. reconstruct antenna patterns from near-field measurements using the radiation centers of the antenna[3] while Tkadlec et al. reconstruct far-field radiation patterns from near-field amplitude measurements using the global particle swarm optimization (PSO).[4] Finally, Rammal et al. reconstructs wide-band–far-field radiation patterns from near-field transient measurements.[5] These transform methods do not directly address pattern reconstruction from limited angular pattern and frequency measurements.

This report proposes a method to reconstruct 2-dimensional (2-D) far-field–wide-band radiation patterns from sparse, randomly distributed measurements using compressive sensing on the radiation-frequency-pattern matrix. This can lead to a new wide-band antenna-measurement method in which the antenna is measured over a small percentage of randomly distributed angles and frequencies; then, reconstructed during postprocessing using compressive sensing. This method would save time and effort by requiring only a small percentage of conventional measurements.

2. Compressive Sensing

Compressive sensing has its roots in transform coding, in which a compressible signal is transformed to a domain where it is sparse (whose basis function contains only a few large coefficients). These large coefficients mostly characterize the

signal, which can be adequately reconstructed by taking the inverse transform of only the large coefficients.

In transform coding, a data set can be represented as

$$\boldsymbol{x} = \boldsymbol{\psi s} \quad , \tag{1}$$

where $\boldsymbol{\psi}$ is an $N \times N$basis matrix, and $\boldsymbol{s}$ is an $N \times 1$ column vector of weighing coefficients. The data set $\boldsymbol{x}$ is said to be K-sparse if it is a linear combination of only K basis vectors.

Transform coding is useful for data storage but assumes the signal is completely known before taking its transform. Compressive sensing begins with an under-sampled signal and attempts to reconstruct the signal using an inversion scheme and an optimization using the ℓ_1-norm.[6]

If $\boldsymbol{y}_{M\times1}$ measurements are taken of the data set $\boldsymbol{x}_{N\times1}$, where $M < N$, the basis matrix $\boldsymbol{\psi}$ can be adjusted for the number of measurements taken by keeping the basis function's rows that only correspond to the measurements taken

$$\boldsymbol{y} = \boldsymbol{\Theta s} \quad , \tag{2}$$

where $\boldsymbol{y}$ are the M measurements taken, $\boldsymbol{\Theta} = \boldsymbol{R\psi}$ is the $M \times N$ basis matrix $\boldsymbol{\psi}$ modified by a matrix $\boldsymbol{R}$, called the measurement matrix (that keeps only the basis functions associated with the measurements), and $\boldsymbol{s}$ is the data set to be reconstructed in the sparse domain. Thus, if the 3rd, 4th, and 7th elements of the signal are measured, the $3 \times N$ matrix $\boldsymbol{\Theta}_{3\times N}$ will consist of the 3rd, 4th, and 7th rows of the discrete Fourier transform (DFT) matrix.

If the basis matrix is orthonormal, its inverse is its transpose, with which we can solve for $\boldsymbol{s}$:

$$\boldsymbol{s} = \boldsymbol{\Theta}^T \boldsymbol{y} \quad . \tag{3}$$

Since the number of measurements is smaller than the data set, or that $M < N$, an infinite amount of solutions exists in the reconstruction of the total data set of length N from M measurements. The signal $\boldsymbol{s}$ is approximated by $\hat{\boldsymbol{s}}$ that is estimated using an iterative ℓ_1-norm minimization routine.[6] The reconstructed data set whose sum of its elements is minimum is chosen, or

$$\hat{\boldsymbol{s}} \quad \text{where} \hat{\boldsymbol{s}} = \|\boldsymbol{s}\|_{min} \quad . \tag{4}$$

The key to the compressive-sensing process is to find and use a transform that will render the signal sparse in the transform space. The most common transforms used are the DFT, the discrete cosine transform (DCT), and the wavelet transform (WT).

Once a transform is chosen, it is cast in discrete matrix form to allow solving for $\boldsymbol{s}$ in Eq. 3. For example, the DFT matrix, $\boldsymbol{\psi}_{N,N}$ can be written as

$$\boldsymbol{\psi}_{N,N} = \frac{1}{\sqrt{N}} \begin{bmatrix} e^{\frac{-j2\pi n_1 k_1}{N}} & \cdots & e^{\frac{-j2\pi n_1 k_N}{N}} \\ \vdots & \ddots & \vdots \\ e^{\frac{-j2\pi n_N k_1}{N}} & \cdots & e^{\frac{-j2\pi n_1 N k_N}{N}} \end{bmatrix} . \quad (5)$$

The $\boldsymbol{\Theta}_{M,N}$ matrix is then inverted and multiplied by the measurements to yield the reconstructed data in the sparse domain. The reconstructed signal $\hat{\boldsymbol{s}}$ is transformed back into the measurement domain using the inverse transform, which in this case is the inverse Fourier transform or inverse cosine transform.

Compressive sensing allows the reconstruction of an$N$-length vector using $M < N$ data points if the vector is compressible; that is, if the vector can be transformed into a domain where its coefficients will be sparse. The amount of data needed to reconstruct a signal is inversely proportional to the compressibility of the signal.

3. Radiation-Frequency Pattern's Reconstruction

Three antennas were modeled with a high-frequency structural simulator (HFSS) to calculate radiation patterns over a relatively wide-band; their radiation-frequency patterns were reconstructed to explore the limits of success of the compressive-sensing method for this application. The first antenna was a pyramidal horn modeled between 1.2 GHz and 1.7 GHz. The second antenna modeled was a Vivaldi antenna whose radiation pattern was calculated between 4 GHz and 8 GHz. The third antenna analyzed was a bicone antenna modeled between 1 GHz and 4 GHz. Two-dimensional radiation patterns were calculated at 1° increments (360 calculation points), with 100 calculations equally spanning the frequency interval specified.

When applying compressive sensing to the reconstruction of antenna radiation-frequency patterns from incomplete angular and frequency calculation points, it was found that the radiation patterns compressed well using a basis function derived from the DFT and the DCT[7] in both the angular and frequency dimensions of the measured data. This compressibility allows reconstruction of the radiation-frequency patterns of the antenna from partial radiation-frequency patterns measured at randomly distributed angles and frequencies. Because the reconstruction of the radiation-frequency pattern is performed in both the angular and frequency dimensions, the radiation pattern is reconstructed at one measured frequency at a time, meaning that each row of the angle-frequency-measurement matrix is reconstructed individually. This concept of parallel compressed sensing was reported by Fang et al.[8] Because the frequency reconstruction of the radiation-

frequency pattern is not dependent on the angular reconstruction, the parallel-reconstruction technique used in this research yields a 1.5-dimensional reconstruction. In this research the number of randomly distributed, calculated points used to reconstruct the radiation-frequency pattern is the same in both the angular and frequency dimensions.

Both the radiation pattern and the frequency behavior of the pattern can be reconstructed sequentially using the same random-frequency calculated points at each angle of measurement (uniform reconstruction) or with different random-frequency calculated points (nonuniform reconstruction). The errors eventually introduced into the radiation-frequency patterns when using a small subset of the total calculated points differ in character depending on whether uniform or nonuniform reconstruction is performed. Reconstruction of the radiation-frequency patterns of the 3 antenna models is performed with the DFT and DCT using uniform and nonuniform random-frequency-measurement distributions, and the results are analyzed to determine the minimum amount of calculated points needed for adequate reconstructions.

3.1 Pyramidal Horn Antenna's Reconstruction

The total electric field, $\boldsymbol{E}_{total}$, radiation-frequency pattern of a pyramidal horn was simulated with HFSS and is presented in Fig. 1. As expected, the mainbeam narrows and the side-lobe levels rise with frequency.

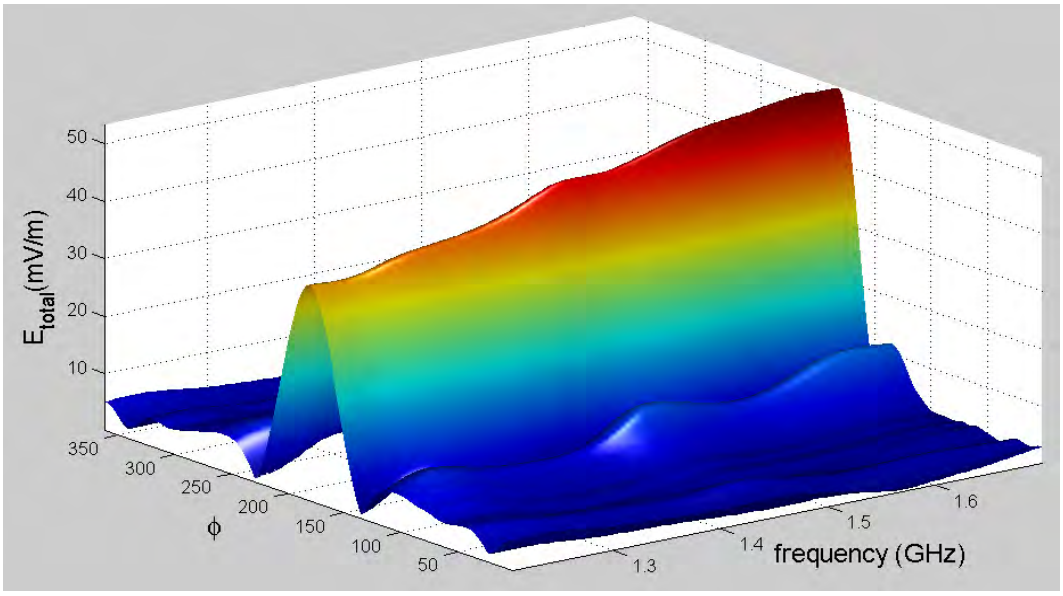

Fig. 1 The radiation-frequency pattern of a pyramidal horn antenna modeled from 1.2 GHz to 1.7 GHz

The pyramidal horn's radiation-frequency pattern is perfectly recreated using 60% of the measured data in both angular and frequency dimensions, regardless of the transform used in the reconstruction. Figure 2 shows the uniform reconstruction of the radiation-frequency pattern. (The black symbols on the reconstructed radiation-frequency pattern's surface are the measurement used in the reconstructions.)

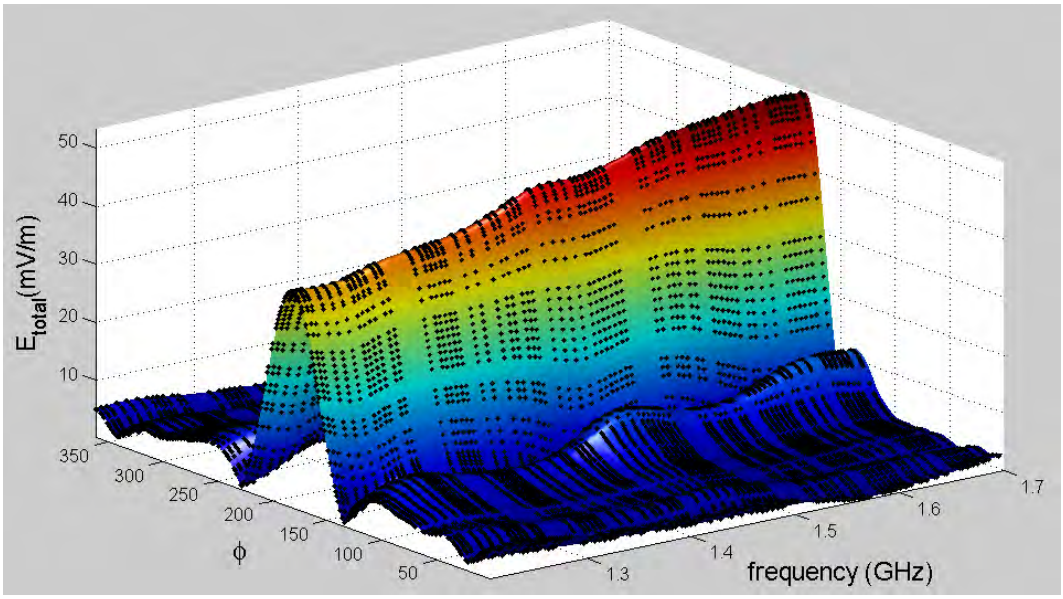

Fig. 2 The uniform compressive-sensing reconstruction of the radiation-frequency pattern of the pyramidal horn antenna using 60% of the calculated points

Figure 3 shows the nonuniform reconstruction of the pyramidal horn antenna's radiation-frequency pattern.

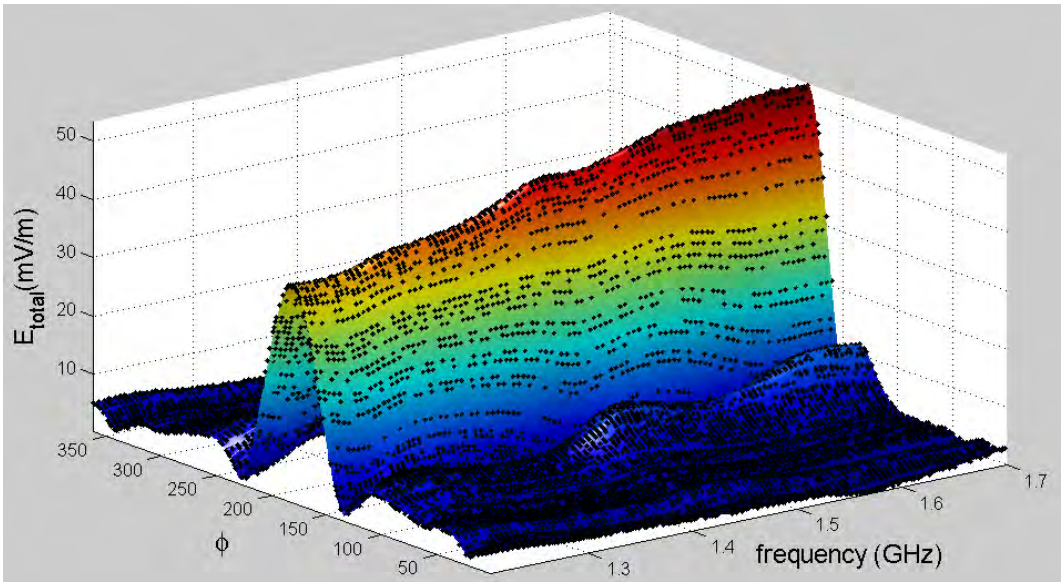

Fig. 3 The nonuniform compressive-sensing reconstruction of the radiation-frequency pattern of the pyramidal horn antenna using 60% of the calculated points

Figures 2 and 3 show the radiation-frequency pattern of the pyramidal horn is recreated very well using 60% of the calculated points and that no difference in reconstruction exists whether the reconstruction was uniform or nonuniform.

Next, the root-mean-square error (RMSE) of the frequency-behavior reconstruction is calculated as a function of number of randomly distributed calculated points. This error analysis is performed for every radiation angle measured, yielding waterfall plots shown in Figs. 4 and 5. Figure 4 shows the RMSE when the reconstruction is performed using the DFT while Fig. 5 shows the RMSE when the DCT is used. Because of the randomness of the frequency calculated points used, the reconstruction error was calculated 10 times and the RMSE curves were averaged over the 10 trials.

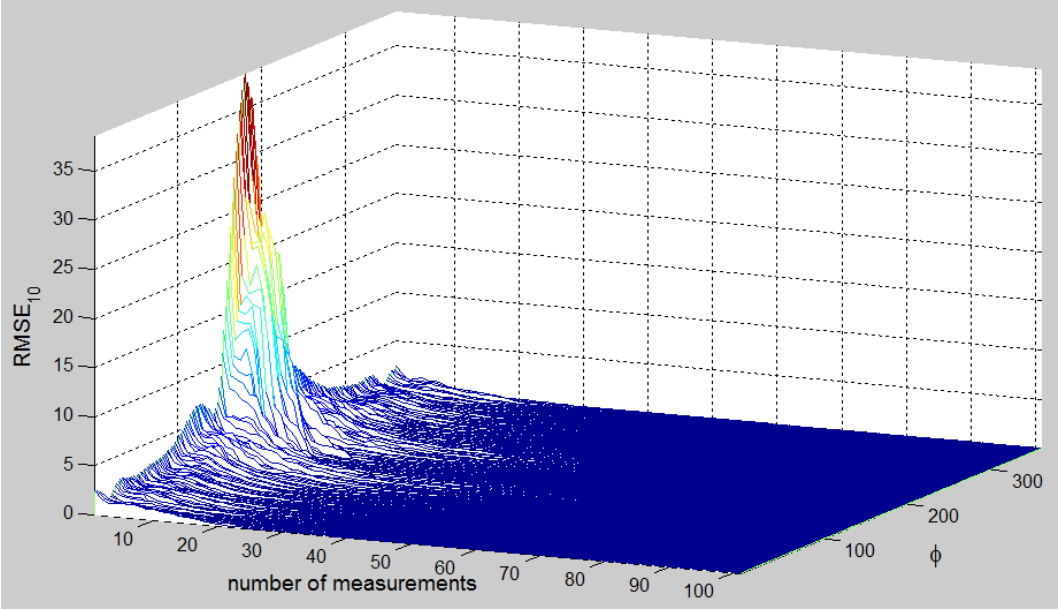

Fig. 4 The average of 10 RMSE calculations of the DFT reconstruction of the pyramidal horn as a function of the number of frequency calculated points used

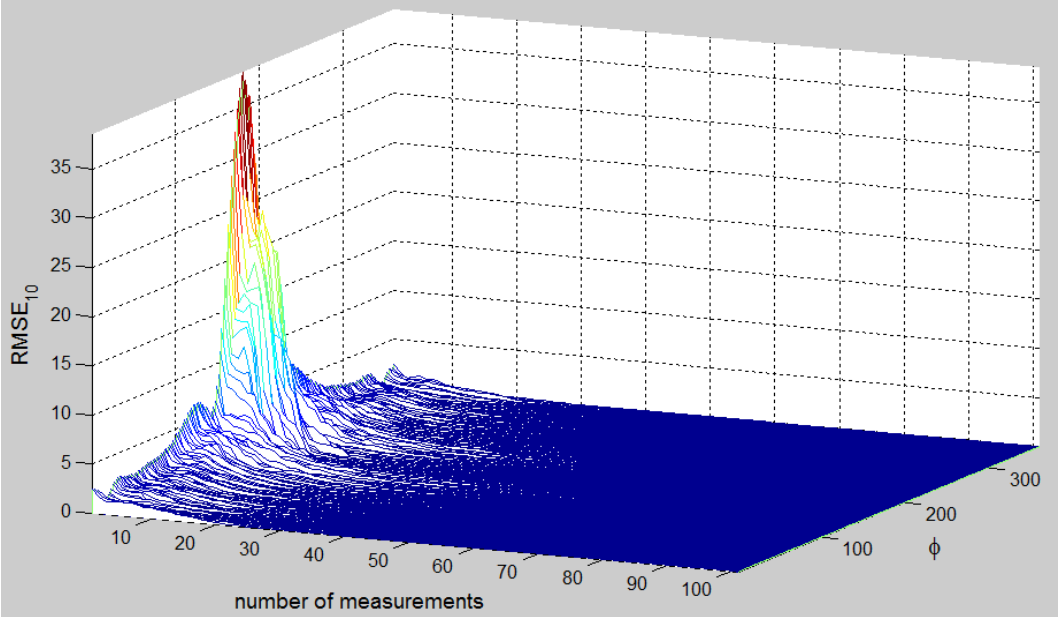

Fig. 5 The average of 10 RMSE calculations of the DCT reconstruction of the pyramidal horn as a function of the number of frequency calculated points used

Figures 4 and 5 show the RMSEs of the reconstructions need about 30% of the randomly distributed frequency calculated points to reconstruct the radiation-frequency pattern of the pyramidal horn antenna. Moreover, it is seen that the DFT and DCT reconstructions converge similarly with the same percentage of randomly distributed calculated points. Using 30% of the randomly distributed frequency calculated points, and comparing the DFT and DCT reconstructions, it was found that the DCT reconstructed the frequency behavior of the radiation-frequency pattern better. The DFT was thus used to compare the uniform and nonuniform reconstructions.

Figures 6 and 7 show the radiation-frequency reconstructions using 30% of the calculated points for both the uniform and nonuniform reconstruction techniques. The DCT is used to reconstruct the frequency behavior while the DFT is used to reconstruct the angular behavior. Interestingly, the error in pattern reconstruction manifests itself differently in the uniform and nonuniform reconstructions. A comparison of Figs. 6 and 7 shows the uniform random distribution reconstructs the horn antenna with less error than the nonuniform random distribution using 30% of the randomly distributed calculated points.

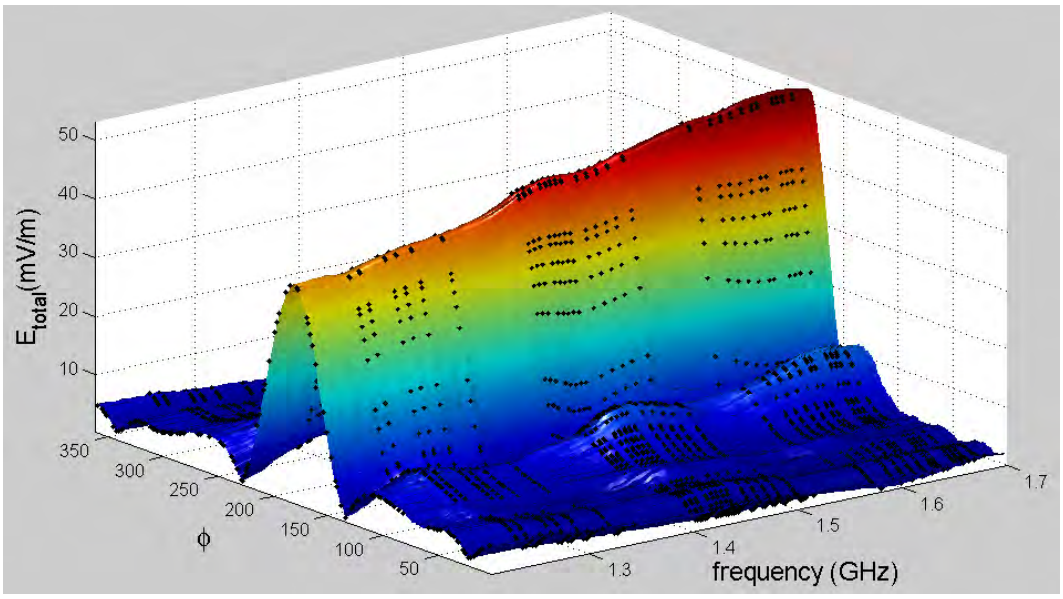

Fig. 6 The uniform DCT compressive-sensing reconstruction of the radiation-frequency pattern of the pyramidal horn antenna using 30% of the calculated points

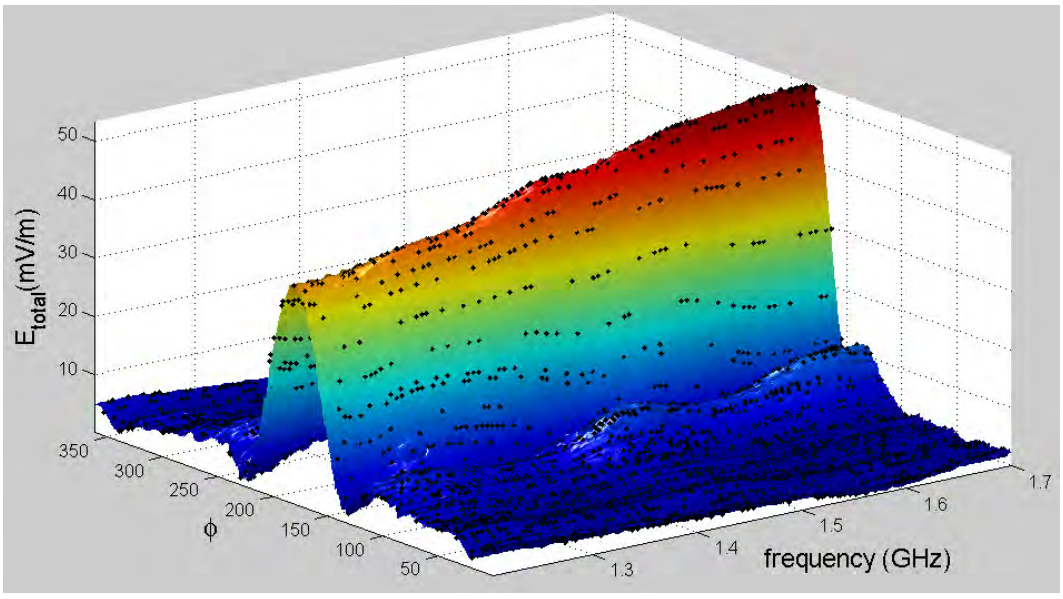

Fig. 7 The nonuniform DCT compressive-sensing reconstruction of the radiation-frequency pattern of the pyramidal horn antenna using 30% of the calculated points

3.2 Vivaldi Antenna's Reconstruction

Next, the E_{total} radiation-frequency pattern of a Vivaldi antenna was modeled with HFSS and reconstructed using the compressive-sensing method. The radiation-frequency pattern of the Vivaldi-antenna model is shown in Fig. 8.

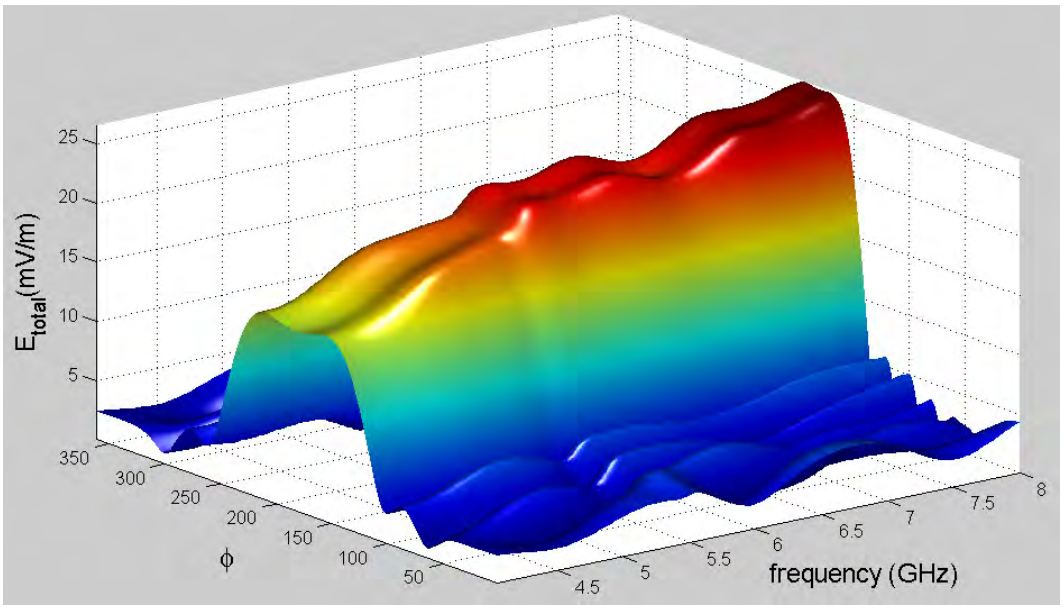

Fig. 8 The radiation-frequency pattern of a Vivaldi antenna modeled from 4 GHz to 8 GHz

The RMSE plot as a function of the percentage of frequency calculated points used for reconstructions using the DFT is shown in Fig. 9. It shows the radiation-frequency pattern of the Vivaldi-antenna model can also be adequately reconstructed using a random distribution of 30% of the calculated points.

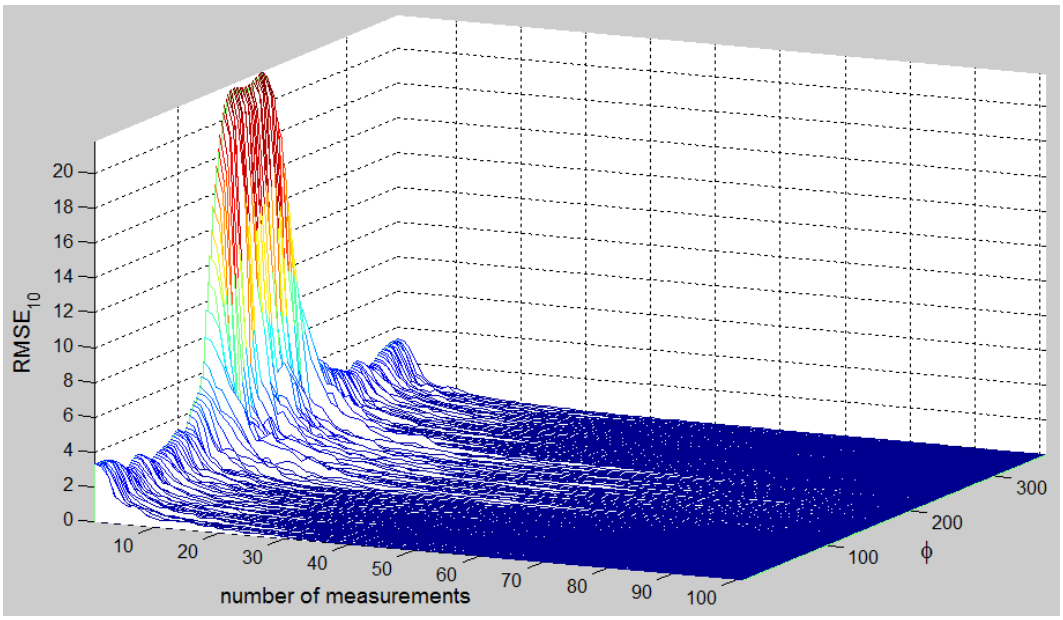

Fig. 9 The average of 10 RMSE calculations of the DFT reconstruction of the Vivaldi antenna as a function of the number of frequency calculated points used

Figure 10 shows the RMSE error of the DCT reconstruction as a function of number of randomly distributed calculated points.

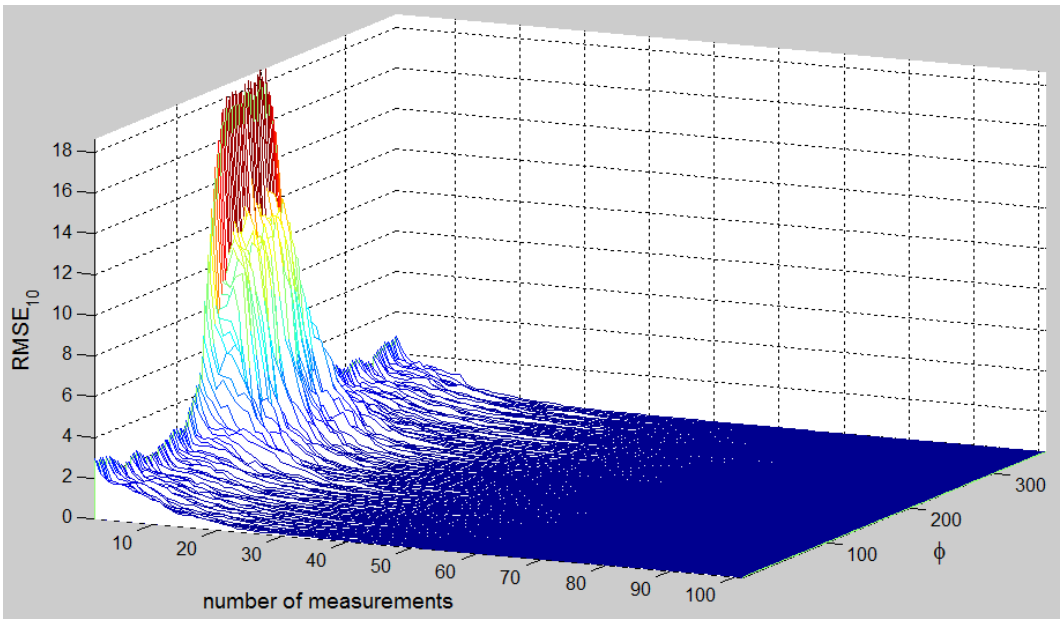

Fig. 10 The average of 10 RMSE calculations of the DCT reconstruction of the Vivaldi antenna as a function of the number of frequency calculated points used

A comparison of Figs. 9 and 10 shows the DFT reconstruction converges with the model with slightly fewer points. Again, the compressive-sensing reconstruction converges to the radiation-frequency pattern when about 30% of the calculated points are used.

The Vivaldi's radiation-frequency pattern is uniformly reconstructed using the DFT with 30% of the randomly distributed calculated points. It is shown in Fig. 11. Superimposed on the reconstruction's surface are the calculated points used for the reconstruction. Again, the angular reconstruction was performed with a DFT while the frequency reconstruction was performed with a DCT.

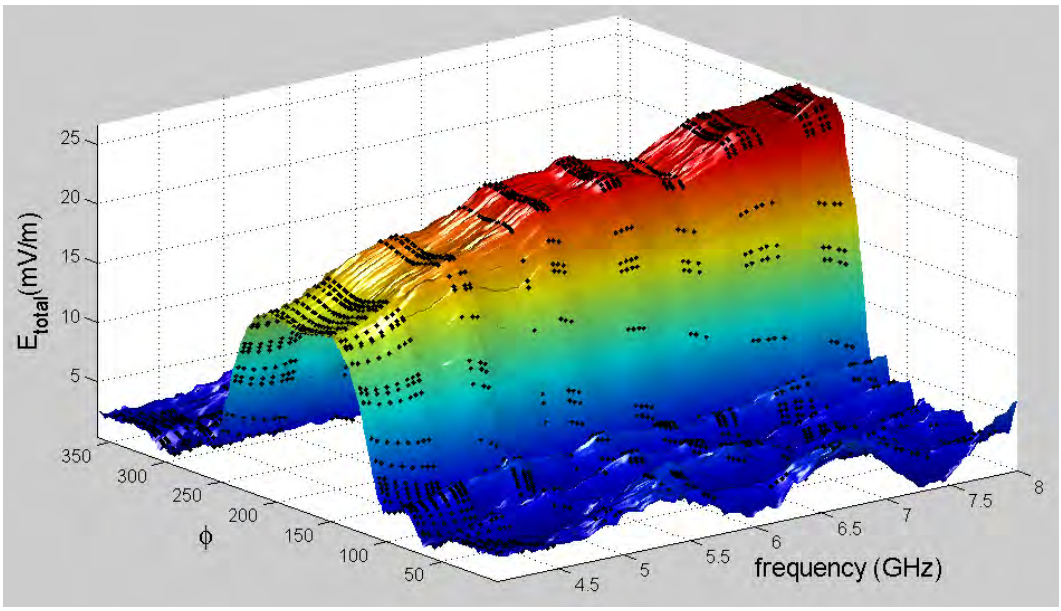

Fig. 11 The uniform DCT reconstruction of the Vivaldi antenna's radiation-frequency pattern using 30% of the randomly distributed calculated points

For comparison, Fig. 12 shows the Vivaldi's radiation-frequency pattern reconstructed nonuniformly using the DFT with 30% of the randomly distributed calculated points. While the errors introduced in the radiation-frequency pattern's uniform and nonuniform reconstructions have different characteristics, both reconstruct the radiation-frequency patterns equally well.

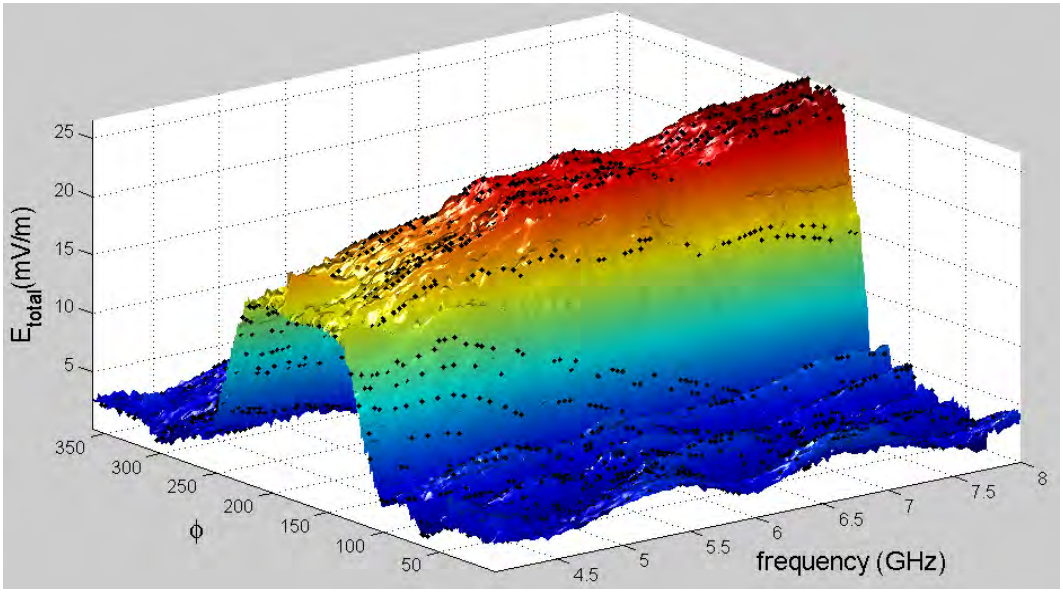

Fig. 12 The nonuniform DCT reconstruction of the Vivaldi antenna's radiation-frequency pattern using 30% of the randomly distributed calculated points

3.3 Bicone Antenna's Reconstruction

Finally, a center-fed bicone antenna was modeled from 1 GHz to 4 GHz and the$\boldsymbol{E}_{total}$ radiation-frequency pattern was calculated. This antenna model was chosen to test the compressive-sensing reconstruction on a radiation-frequency pattern that varies substantially over the frequency band considered. Figure 13 shows the radiation-frequency pattern of the bicone antenna. As expected, the antenna starts with 2 lobes at 1 GHz and ends with 4 lobes at 4 GHz.

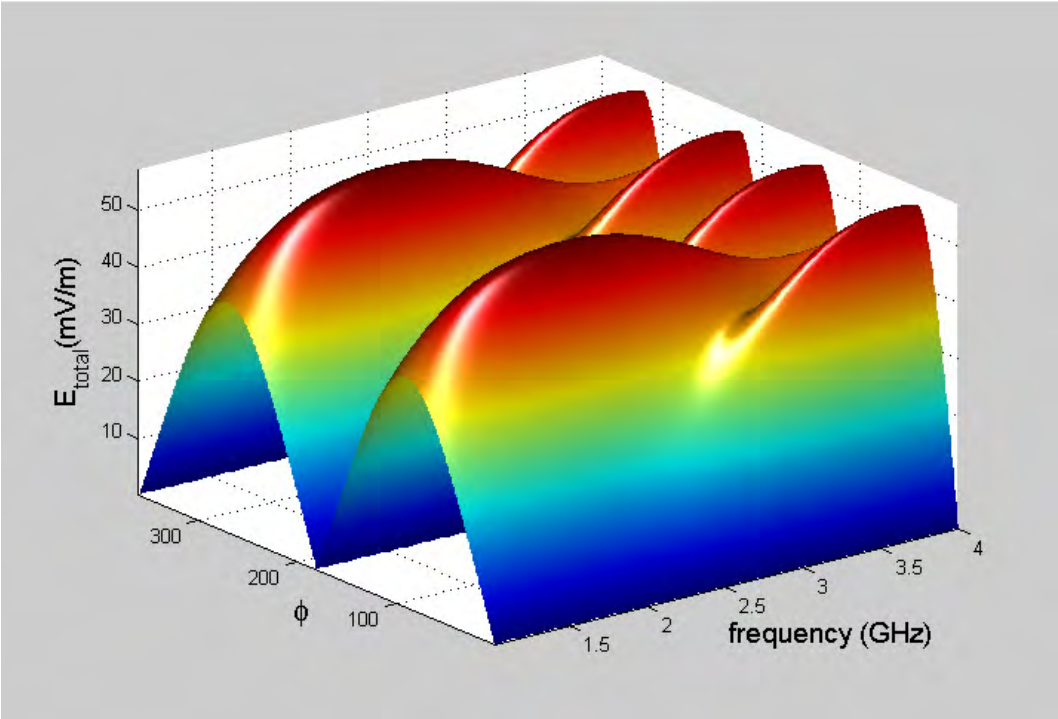

Fig. 13 The radiation-frequency pattern of a bicone antenna from 1 GHz to 4 GHz

Figure 14 shows the average of 10 RMSE calculations of the reconstruction of the bicone antenna's radiation-frequency pattern using the DFT as a function of frequency calculated points used. Figure 15 shows the average of 10 RMSE calculations of the reconstruction of the bicone antenna's radiation-frequency pattern using the DCT. As with the pyramidal and Vivaldi antennas' radiation-frequency patterns, the bicone requires about 30% of randomly distributed calculated points to reconstruct. Figures 16 and 17 suggest the DFT reconstruction also converges to the model with fewer randomly distributed frequency calculation points.

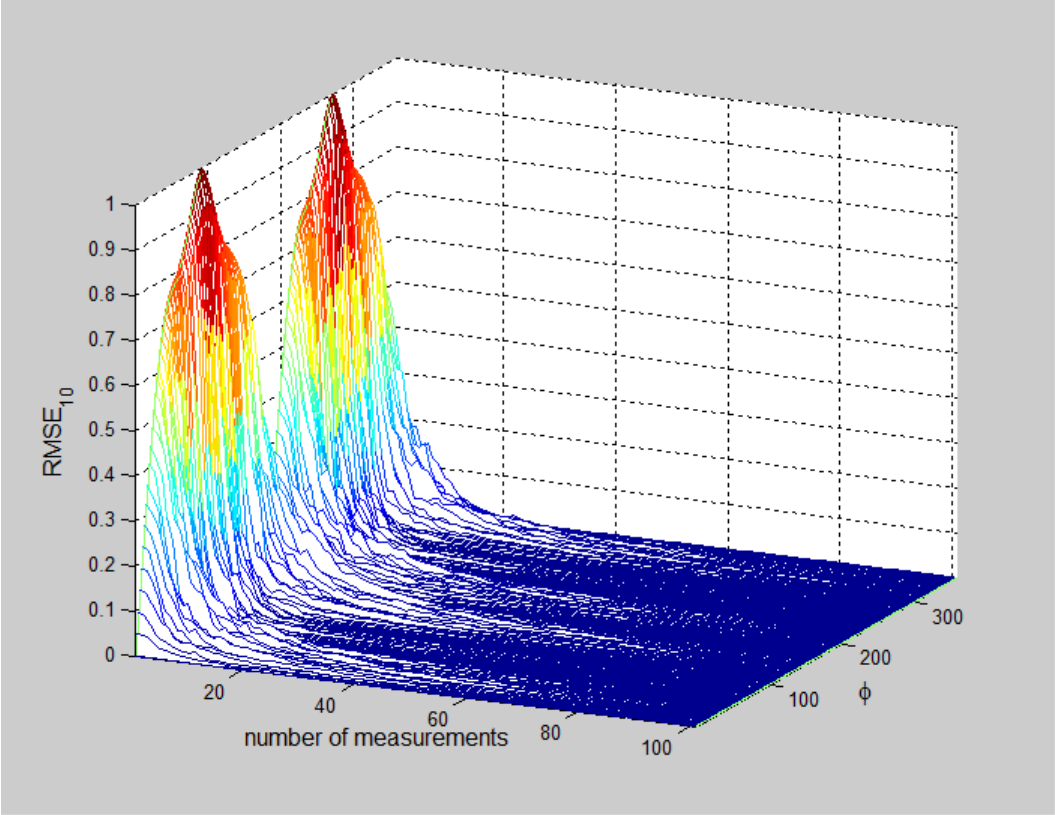

Fig. 14 The average of 10 RMSE calculations of the DFT reconstruction of the bicone antenna as a function of the number of frequency calculated points used

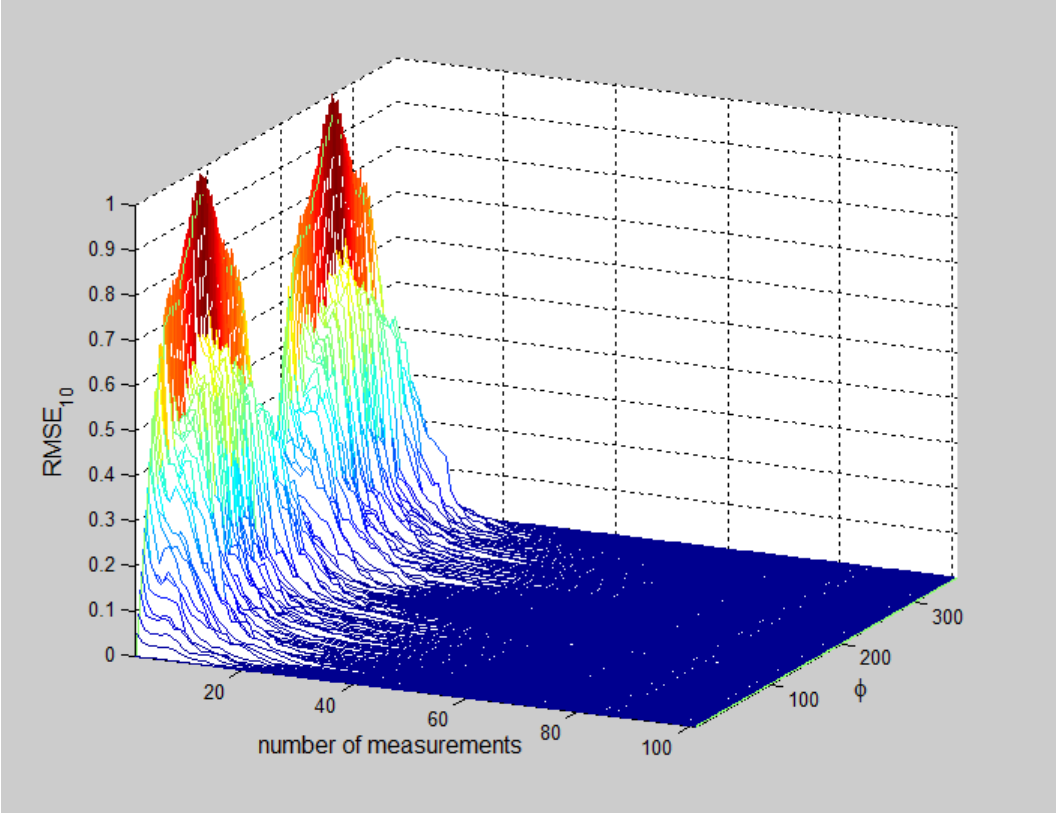

Fig. 15 The average of 10 RMSE calculations of the DCT reconstruction of the bicone antenna as a function of the number of frequency calculated points used

Figures 16 and 17 show the uniform and nonuniform reconstruction of the bicone antenna using 30% of the randomly distributed calculated points, respectively. As with the 2 previous antenna models, the reconstruction was performed using the DFT for the angular reconstruction and the DCT for the frequency reconstruction. The Figures show the uniform reconstruction is slightly efficient at reconstructing the radiation-frequency pattern of a bicone antenna over a wide frequency range.

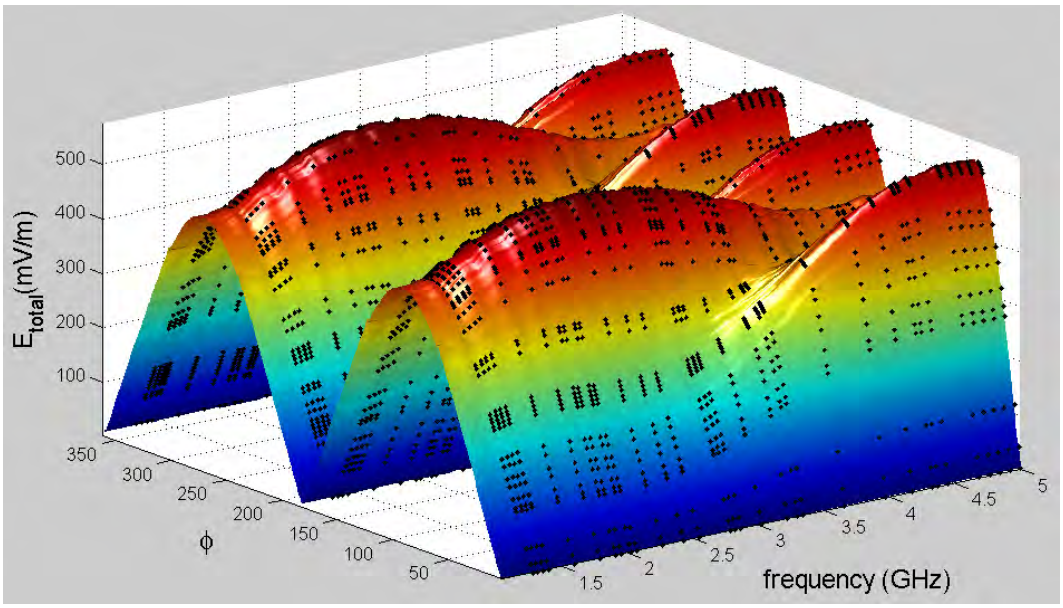

Fig. 16 The uniform DCT reconstruction of the radiation-frequency pattern of bicone antenna using 30% of the randomly distributed calculated points

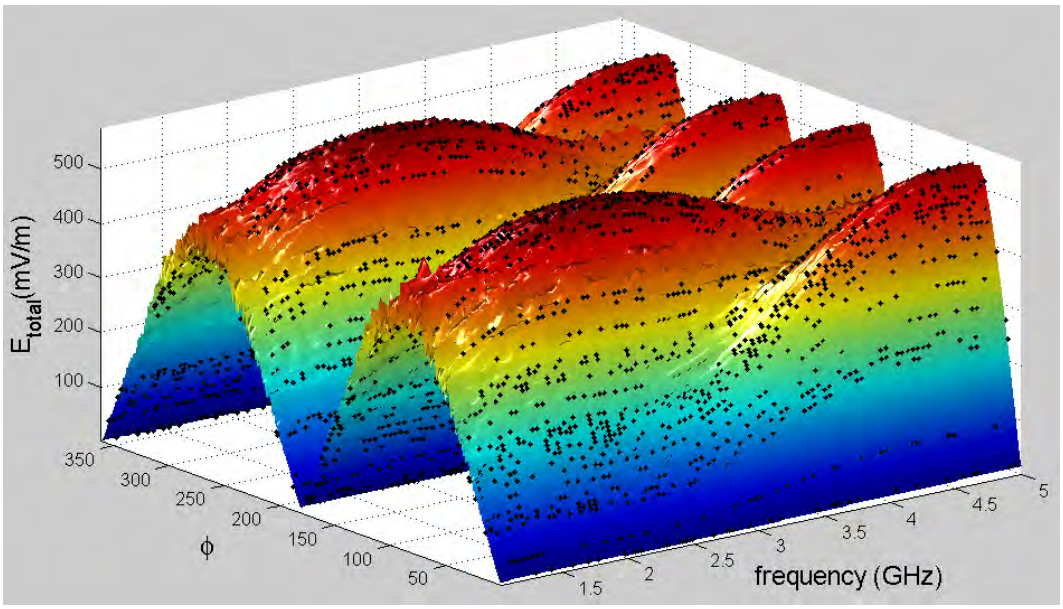

Fig. 17 The nonuniform DCT reconstruction of the radiation-frequency pattern of bicone antenna using 30% of the randomly distributed calculated points

4. Conclusions

The compressive sensing has been demonstrated to reconstruct radiation-frequency patterns of various modeled wide-band antennas. The success of reconstructing the patterns of 3 antenna models was analyzed using the DFT versus the DCT. The relative successes of using uniform versus nonuniform reconstructions were

compared for each antenna. The RMSEs of the frequency reconstructions were calculated as a function of the number of calculated points used, to show the convergence of the reconstruction over all radiation angles.

The reconstruction approach that seemed to work best for the 3 antenna models considered was a hybridized transform approach in which the DFT was used to reconstruct the angular component and the DCT was used to reconstruct the frequency dependence of the radiation-frequency pattern. A comparison of the RMSE waterfall plots shows the approximate percentage of frequency calculated points needed to reconstruct the radiation-frequency pattern—that percentage being applied to both the angular and frequency component of the reconstruction. For a given percentage of calculated points used for the reconstruction, it was found that the DFT was better suited to reconstruct the angular dependence of the pattern while the DCT worked better to reconstruct the frequency component of the radiation-frequency patterns of the 3 antenna models considered.

Comparison of the uniform and nonuniform reconstruction methods did not yield a solid trend: The pyramidal horn and bicone antennas' radiation-frequency-pattern reconstruction favored uniform reconstruction while the Vivaldi antenna's radiation-frequency pattern reconstruction appeared to favor nonuniform reconstruction. It is noted, however, that due to the random nature of the calculated points chosen to perform the reconstruction, that different reconstruction trials yield different results. Therefore, even though the characteristics of the reconstruction errors differ substantially between uniform and nonuniform reconstruction, each method may yield better results for a given percentage of calculated points used.

In this study, the 3 antennas' radiation-frequency patterns reconstructed adequately using 30% of the modeled calculations. The reduction of required calculated points to the 30% needed to reconstruct the bicone antenna is notable due to the large change in radiation pattern over the frequency band considered (2 lobes at the lower band-edge and 4 lobes at the upper band-edge). One observed trend in the antennas' analyses was that the number of randomly distributed calculated points required to recreate the radiation-frequency pattern increased with the complexity of the radiation-frequency pattern of the antenna.

Because some of the trends in the 3 antennas' analyses are consistent—angular reconstruction is better performed with the DFT, frequency reconstruction is better performed with the DCT—an algorithm can be designed that will reconstruct the radiation-frequency pattern of an antenna using a small percentage of randomly distributed calculated points. This algorithm could have a safety margin for the unknown complexity of the pattern; for example, using 50% of the calculated points to reconstruct the radiation-frequency pattern of an antenna without having *a priori*

knowledge of the complexity of the pattern. In this way, use of a compressed-sensing algorithm to reconstruct a radiation-frequency pattern from a limited number of randomly distributed points could save half of the measurement time of a wide-band antenna pattern.

5. References

1. Miller EK. Using adaptive estimation to minimize the number of samples needed to develop a radiation or scattering pattern to a specified uncertainty. Appl Comp Electro Soc J. 2002;17(3):176–186.
2. Werner DH, Allard RJ. The simultaneous interpolation of antenna radiation patterns in both the spatial and frequency domains using model-based parameter estimation. IEEE Trans Ant Prop. 2000;48(3):383–392.
3. Martí-Canales J, Lighart LP. Reconstruction of measured antenna patterns and related time-varying aperture fields. IEEE Trans Ant Prop. 2004;52(11):3143–3147.
4. Tkadlec R, Nováček Z. Radiation pattern reconstruction from the near-field amplitude measurement on two planes using PSO. Radio Eng. 2005;14(4):63–67.
5. Rammal R, Lalande M, Martinod E, Feix N, Jouvet M, Andrieu J, Jecko B. Far-field reconstruction from transient near-field measurement using cylindrical modal development. Int J Ant Prop. 2009;2009:1–7.
6. Baraniuk RG. Compressive sensing. IEEE Sig Proc Mag. 2007;24(4):118–120,124.
7. Verdin B, Debroux P. Sparse matrix motivated reconstruction of far-field radiation patterns. IEEE Ant Prop Soc. Forthcoming 2015.
8. Fang H, Vorobyov SA, Jiang H, Taheri O. Permutation meets parallel compressed sensing: how to relax restricted isometry property for 2D sparse signals. IEEE Trans Sig Proc. 2014;62(1):196–210.

List of Symbols, Abbreviations, and Acronyms

DCT	discrete cosine transform
DFT	discrete Fourier transform
HFSS	high-frequency structural simulator
MBPE	model-based parameter estimation
PSO	particle swarm optimization
RMSE	root-mean-square error
2-D	2-dimensional
WT	wavelet transform

1 (PDF)	DEFENSE TECHNICAL INFORMATION CTR DTIC OCA
2 (PDF)	DIRECTOR US ARMY RSRCH LAB RDRL CIO LL IMAL HRA MAIL & RECORDS MGMT
1 (PDF)	GOVT PRINTG OFC A MALHOTRA
1 (WORD VERSION)	US ARMY RSRCH LAB ATTN RDRL SLE MARISSA WITHERS BLDG 1624 RM 210 WSMR NM 88002-5513
1 (PDF)	RDRL-SLE-E P DEBROUX